Design of a Viscous Ring Nutation Damper for a Freely Precessing Body

C. O. Chang* and C. S. Chou*
National Taiwan University, Taipei, Taiwan, Republic of China
and
S. Z. Wang†
Chung Shan Institute of Science and Technology, Long Tang, Taiwan, Republic of China

A ring damper partially filled with mercury for removing the wobble motion of a freely precessing body is analyzed. Coupled equations of motion of the rotor and mercury are derived in terms of Euler parameters and quasicoordinates for the purposes of computational efficiency and singularity-free solution when the nutation angle approaches zero. An experiment is made to verify the theoretical solution of the nutation angle obtained by numerical integration of the equations of motion. The best choice of parameters of the damper is obtained by solving a minimum-time optimization problem that minimizes the time elapsed in the nutation-synchronous mode as well as the residual nutation angle in the spin-synchronous mode. The results show that the decay of the nutation angle can be accelerated to a great extent if the damper is properly designed.

Introduction

WHEN a moment-free inertially symmetric spinning body is subjected to an impulsive torque, i.e., a suddenly applied torque with brief duration, it will result in coning (or precession) motion of the spin axis about the angular momentum vector (which is fixed in space in the absence of subsequent external torques). The ring damper, partially filled with mercury and mounted on the spinning body (or the rotor of a gyroscope), has the effect in reducing the cone angle (or nutation angle), so it has been extensively used in satellites to keep their orientation and in gyroscopic seekers of missiles to confirm precise tracking. The behavior of the nutation angle can be characterized by three distinct modes, namely the nutation-synchronous mode, the spin-synchronous mode,[1-3] and the fluid mode.[4,5] The nutation- and spin-synchronous modes occur in the case for which the rotor is in motion with large nutation angle after application of an impulsive torque. The shape of mercury inside the ring remains crescent. This crescent mercury behaves as a rigid slug. It first goes round and round with respect to the ring damper in the nutation-synchronous mode and then oscillates with small amplitude about the nutation plane in the spin-synchronous mode. The fluid mode occurs in the case where the rotor is in motion with small nutation angle and the shape of mercury is annulus-like.

Bhuta and Koval[4] and Miles[5] analyzed the fluid mode by using the energy-sink approximation which assumes that the energy dissipation rate of the fluid equals the rate of kinetic energy change of the rotor. Cartwright et al.[1] modeled the crescent viscous fluid as a point mass and analyzed the nutation-synchronous mode but failed to analyze the spin-synchronous mode. By considering the rotational inertia of the fluid, Alfriend[2] and Alfriend and Spencer[3] modeled the crescent fluid as a rigid slug of finite length and analyzed both the nutation-synchronous and spin-synchronous modes. By defining a small parameter ϵ that is the ratio of the moment of inertia of the slug about the spin axis to the transverse moment of inertia of the rotor, Alfriend developed approximate governing equations obtained by simplifying the equations of motion up to the terms of power of ϵ^0. The approximate solutions of Cartwright et al.[1] and Alfriend[2] provide the preliminary physical understanding of damper performance. However, it may be due to the oversimplifying in equations of motion that the expression for the nutation angle in the spin synchronous mode obtained by Alfriend [Eq. (24) of Ref. 2] cannot interpret the existence of the residual nutation angle.

In the present paper, the nutation-synchronous and spin-synchronous modes of a gyroscopic seeker, which carries a ring damper partially filled with mercury and spins at a high speed of 70 Hz, are analyzed. The rotor is made of magnet and connected by a ball joint to the main structure of a missile fixed in space. The gyroscope is so designed that its center of mass coincides with the center of the ball joint. The spin axis of the rotor is expected to aim at the target. Once the optical detector inside the rotor detects the deviation of the target, the rotor is driven immediately to lock it by an impulsive torque generated by the coil surrounding the rotor. From our experimental observation, the shape of the mercury inside the ring looks like a crescent as shown in Fig. 1, so the mercury in the ring is modeled as a rigid slug in our analysis. Central to this paper is the analysis of the effect of the parameters of the damper on the decay of wobble motion of the rotor and the optimal design of the damper based on optimization techniques. Complete nonlinear equations of motion are adopted here on the parameter analysis, since the use of simplified equations of motion may lose something important as has been mentioned above. Coupled equations of motion are

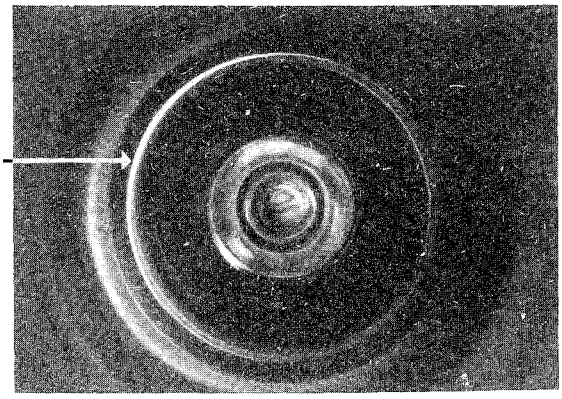

Fig. 1 Snapshot of the mercury in the ring.

Received Oct. 5, 1989; revision received March 27, 1990; accepted for publication Aug. 6, 1990.

*Associate Professor, Institute of Applied Mechanics.
†Assistant Researcher.

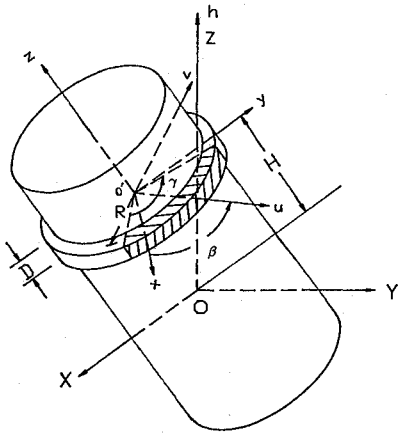

Fig. 2 Idealized rotor and mercury-filled ring.

derived in terms of quasicoordinates in order to reduce the number of equations of motion as well as the number of sensitivity equations needed for evaluating the gradients of the state variables with respect to the design variables in the optimization technique we used. The shearing force between the rotor and the mercury is obtained by assuming a steady turbulent flow over a straight pipe. The good agreement between the theoretical prediction and the experimental result on the decay time of the nutation angle in nutation-synchronous mode validates our modeling. Since the effects on the decay of nutation angle and the average residual nutation angle in the spin-synchronous mode are quite different for various parameters of the damper according to our numerical results, the optimization problem which minimizes the decay time in the nutation-synchronous mode and the average residual nutation angle in the spin-synchronous mode is selected as a means of finding the best set of parameters of the damper. The logical constraints are used to overcome the difficulty in finding the transition time from the nutation-synchronous mode to the other. The direct differentiation of the complete nonlinear equations of motion with respect to the design variables is adopted here to evaluate the gradients of the state variables.

Dynamics Analysis

The idealized rotor and mercury-filled ring are shown in Fig. 2. Let H denote the height of the ring damper to the point O which is the center of mass of the gyroscope, ΔR and D the width and depth of the rectangular cross section of the ring, respectively, γ the angle of fill of the mercury in the ring, and R the mean radius of the ring. The angular momentum vector of the gyroscope $\boldsymbol{h}$ about the point O is fixed in space since the gyroscope is free after application of an impulsive torque. Let the Cartesian coordinate system X, Y, Z be the inertial reference frame with origin coinciding with the mass center of the gyroscope and the Z axis parallel to $\boldsymbol{h}$. The Cartesian coordinate system x, y, z is fixed on the rotor with origin coinciding with the center of the ring o' and xy plane lying on the plane of the ring damper. The system u, v, z is fixed on the slug with the u axis passing through its center of mass. The angle β measured from the x axis to the u axis is the angular displacement of the slug relative to the rotor.

The Euler's parameters[6,7] $\boldsymbol{p} = (e_0, e_1, e_2, e_3)^T$, which are a quaternion, are introduced here instead of Eulerian angles to describe the orientation of the rotor with respect to the system X, Y, Z. The reason is that quaternions have no inherent geometrical similarities and no singularities in kinematic differential equations, but Eulerian angles have. In terms of Euler's parameters, the rotational transformation matrix $\boldsymbol{A}$ from system X, Y, Z to system x, y, z can be expressed as the product of two 3×4 matrices[8] as

$$\boldsymbol{A} = \boldsymbol{E}\boldsymbol{G}^T \tag{1}$$

where

$$\boldsymbol{E} = \begin{bmatrix} -e_1 & e_0 & -e_3 & e_2 \\ -e_2 & e_3 & e_0 & -e_1 \\ -e_3 & -e_2 & e_1 & e_0 \end{bmatrix}$$

$$\boldsymbol{G} = \begin{bmatrix} -e_1 & e_0 & e_3 & e_2 \\ -e_2 & -e_3 & e_0 & -e_1 \\ -e_3 & e_2 & -e_1 & e_0 \end{bmatrix} \tag{2}$$

These four Euler's parameters are not independent, and they satisfy the following constraint equation:

$$\boldsymbol{p}^T \cdot \boldsymbol{p} = 1 \tag{3}$$

Let $\omega = (\omega_X, \omega_Y, \omega_Z)^T$ and $\omega' = (\omega_x, \omega_y, \omega_z)^T$ denote the angular velocity of the rotor in the X, Y, Z system and the x, y, z system, respectively. They satisfy the following kinematic equations:

$$\omega = 2\boldsymbol{E}\dot{\boldsymbol{p}} = -2\dot{\boldsymbol{E}}\boldsymbol{p} \tag{4}$$

$$\omega' = 2\boldsymbol{G}\dot{\boldsymbol{p}} = -2\dot{\boldsymbol{G}}\boldsymbol{p} \tag{5}$$

Multiplying both sides of Eq. (5) by $\boldsymbol{G}^T$, and using Eq. (3) and the following identity,

$$\boldsymbol{G}^T\boldsymbol{G} = -\boldsymbol{p}\boldsymbol{p}^T + \boldsymbol{I}_{(4\times 4)} \tag{6}$$

one obtains

$$\dot{\boldsymbol{p}} = \tfrac{1}{2}\boldsymbol{G}\omega' \tag{7}$$

Equations of Motion

The inertia matrix $\boldsymbol{I}_g$ of the rotor about the point O in the x, y, z system is

$$\boldsymbol{I}_g = \text{diag}\,(J_1, J_2, J_3)$$

where J_1, J_2, and J_3, are the moments of inertia of the rotor about the x, y, z axes. The inertia matrix $\boldsymbol{I}_m$ of the mercury about the point o in the u, v, z system is

$$\boldsymbol{I}_m = \begin{bmatrix} I_1 & 0 & -I_4 \\ 0 & I_2 & 0 \\ -I_4 & 0 & I_3 \end{bmatrix}$$

where the values of I_1, I_2, I_3, and I_4 are given in Appendix A. The kinetic energy T_g of the rotor is

$$T_g = \tfrac{1}{2}\omega'^T \boldsymbol{I}_g \omega'$$

The kinetic energy T_m of the mercury is

$$T_m = \tfrac{1}{2}[\omega_x, \omega_y, \omega_z + \dot{\beta}]\boldsymbol{B}^T\boldsymbol{I}_m\boldsymbol{B}[\omega_x, \omega_y, \omega_z + \dot{\beta}]^T$$

where $\boldsymbol{B}$ is the transformation matrix from system x, y, z to system u, v, z. The gravitational potential V_m of the mercury is

$$V_m = -m\boldsymbol{g}^T\boldsymbol{A}^T\boldsymbol{B}^T(RK, 0, a)^T$$

where $K = (\sin\gamma/2)/(\gamma/2)$, $\boldsymbol{g}[= (g_X, g_Y, g_Z)^T]$ is the gravity with components parallel to X, Y, Z. Using the Lagrange multiplier method, the equations of motion of the gyroscope are

$$\frac{\mathrm{d}}{\mathrm{d}t}\left(\frac{\partial L}{\partial \dot{\boldsymbol{p}}}\right) - \frac{\partial L}{\partial \boldsymbol{p}} = Q_P + \lambda \boldsymbol{p} \tag{8}$$

$$\frac{d}{dt}\left(\frac{\partial L}{\partial \dot{\beta}}\right) - \frac{\partial L}{\partial \beta} = Q_\beta \tag{9}$$

$$\boldsymbol{p}^T \cdot \boldsymbol{p} = 1$$

where $L = T_g + T_m - V_m$ is the Lagrangian of the gyroscope, λ is the Lagrange multiplier due to the constraint Eq. (3), Q_P is the generalized force resulting from the gravitational force of the mercury, and Q_β is the generalized force due to the frictional force between the mercury and the wall of the ring. The above equations of motion are five nonlinear second-order ordinary differential equations and one nonlinear algebraic equation for six unknowns, i.e., $\boldsymbol{p}$, β, and λ. In order to avoid solving the λ and the constraint equation, as well as to reduce the number of governing equations, the arguments $\dot{\boldsymbol{p}}$ in L are replaced by the quasicoordinates ω'. Thus, $L(\boldsymbol{p}, \beta, \dot{\boldsymbol{p}}, \dot{\beta})$ becomes $\bar{L}(\boldsymbol{p}, \beta, \omega', \dot{\beta})$. Using the chain rule, one has

$$\frac{\partial L}{\partial \dot{p}_i} = \frac{\partial \bar{L}}{\partial \omega_j'} \frac{\partial \omega_j'}{\partial \dot{p}_i} \tag{10}$$

$$\frac{\partial L}{\partial p_i} = \frac{\partial \bar{L}}{\partial \omega_j'} \frac{\partial \omega_j'}{\partial p_i} + \frac{\partial \bar{L}}{\partial p_i} \tag{11}$$

where $\dot{p}_i$ and p_i are the ith elements of $\dot{\boldsymbol{p}}$ and $\boldsymbol{p}$, respectively, and ω_j' is the jth element of the vector ω'. From Eq. (5) and the following identity,

$$\tilde{\omega}' = 2\boldsymbol{G}\dot{\boldsymbol{G}}^T = -2\dot{\boldsymbol{G}}\boldsymbol{G}^T \tag{12}$$

where

$$\tilde{\omega}' = \begin{bmatrix} 0 & -\omega_z & \omega_y \\ \omega_z & 0 & -\omega_x \\ \omega_y & \omega_x & 0 \end{bmatrix}$$

one obtains

$$\frac{\partial L}{\partial \dot{\boldsymbol{p}}} = 2\boldsymbol{G}^T \frac{\partial \bar{L}}{\partial \omega'} \tag{13}$$

$$\frac{\partial L}{\partial \boldsymbol{p}} = -2\dot{\boldsymbol{G}}^T \frac{\partial \bar{L}}{\partial \omega'} + \frac{\partial \bar{L}}{\partial \boldsymbol{p}} \tag{14}$$

From Eqs. (13) and (14), Eq. (8) can be rewritten as

$$2\boldsymbol{G}^T \frac{d}{dt}\left(\frac{\partial \bar{L}}{\partial \omega'}\right) + 4\boldsymbol{G}^T \frac{\partial \bar{L}}{\partial \omega'} - \frac{\partial \bar{L}}{\partial \boldsymbol{p}} = Q_P + \lambda \boldsymbol{p} \tag{15}$$

Premultiplication of Eq. (15) by $\boldsymbol{G}$ and using two identities, i.e., $\boldsymbol{G}\boldsymbol{G}^T = \boldsymbol{I}$ and $\boldsymbol{G}\boldsymbol{p} = 0$, one has

$$\frac{d}{dt}\left(\frac{\partial \bar{L}}{\partial \omega'}\right) + \tilde{\omega}' \frac{\partial \bar{L}}{\partial \omega'} - \frac{1}{2}\boldsymbol{G}\frac{\partial \bar{L}}{\partial \boldsymbol{p}} = \frac{1}{2}\boldsymbol{G}Q_P \tag{16}$$

The mechanical power is invariant under coordinate transformation, so

$$\dot{\boldsymbol{p}}^T Q_P = \omega'^T M' \tag{17}$$

where M' is the generalized force vector in the x, y, z coordinate system. Substituting Eq. (5) into Eq. (17) for ω', one has

$$M' = \tfrac{1}{2}\boldsymbol{G}Q_P \tag{18}$$

Then the equations of motion can be recast in the following form:

$$\frac{d}{dt}\left(\frac{\partial \bar{L}}{\partial \omega'}\right) + \tilde{\omega}' \frac{\partial \bar{L}}{\partial \omega'} - \frac{1}{2}\boldsymbol{G}\frac{\partial \bar{L}}{\partial \boldsymbol{p}} = M' \tag{19}$$

$$\frac{d}{dt}\left(\frac{\partial \bar{L}}{\partial \dot{\beta}}\right) - \frac{\partial \bar{L}}{\partial \beta} = Q_\beta \tag{20}$$

$$\dot{\boldsymbol{p}} = \frac{1}{2}\boldsymbol{G}^T\omega'$$

The mercury mass is assumed to be sufficiently small in comparison with the mass of the rotor. If the gravitational effect of the mercury is neglected, $\bar{L}$ does not contain the $\boldsymbol{p}$; then only Eqs. (19) and (20) are needed to be solved. Rearranging Eqs. (19) and (20) in the form of first-order differential equations, one has

$$\begin{bmatrix} & & & -I_4\cos\beta & 0 \\ & [BI_mB^T + I_g]_{(3\times 3)} & & -I_4\sin\beta & 0 \\ & & & I_3 & 0 \\ -I_4\cos\beta & -I_4\sin\beta & I_3 & I_3 & 0 \\ 0 & 0 & 0 & 0 & 1 \end{bmatrix}_{(5\times 5)} \begin{pmatrix} \dot{\omega}_x \\ \dot{\omega}_y \\ \dot{\omega}_z \\ \dot{z}_2 \\ \dot{z}_1 \end{pmatrix} = \begin{pmatrix} f_1 \\ f_2 \\ f_3 \\ f_4 \\ z_2 \end{pmatrix} \tag{21}$$

where $z_1 = \beta$, $z_2 = \dot{\beta}$; f_1, f_2, f_3, and f_4 are given in Appendix B. Note that the constraint Eq. (3) and the unknown λ have been eliminated in the new set of equations of motion.

Frictional Force

Since the shear stress is a linear function of the gradients of velocities with respect to spatial coordinates from the viewpoint of viscous fluid mechanics, we assumed that the frictional force F_D between the mercury and the wall of the ring is proportional to their relative velocity; i.e., $F_D = C_d R\dot{\beta}$. Using the principle of virtual work, one can obtain the generalized force resulting from F_D as

$$Q_\beta = -C_d R^2 \dot{\beta} \tag{22}$$

The equivalent Reynolds number[10] of a straight rectangular pipe is $Re = 2\Delta R D R\dot{\beta}/[(\Delta R + D)\nu]$, where ν is the kinematic viscosity. Since the cross-sectional area of the ring is small and the spin rate of the rotor is high in our case, the magnitude of the Reynolds number is of order 10^4 on an average. So the evaluation of shear stress from turbulent flow must be considered. For the turbulent flow, the shear stress τ_0 on the wall of a straight pipe with circular cross section is[11]

$$\tau_0 = 0.0791 Re^{-1/4}(\tfrac{1}{2}\rho U_m^2) \tag{23}$$

where ρ is the density of mercury and U_m is the average flow velocity ($U_m \approx R\dot{\beta}$). Considering the effect of the curved pipe with circular cross section, Eq. (23) is modified as[11]

$$(\tau/\tau_0) = 1 + 0.075 Re^{1/4}(d/2R)^{1/2} \tag{24}$$

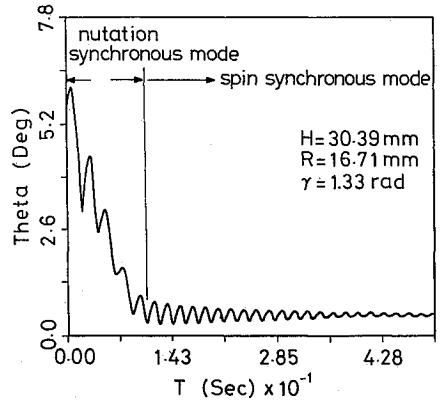

Fig. 3 Time history of the nutation angle.

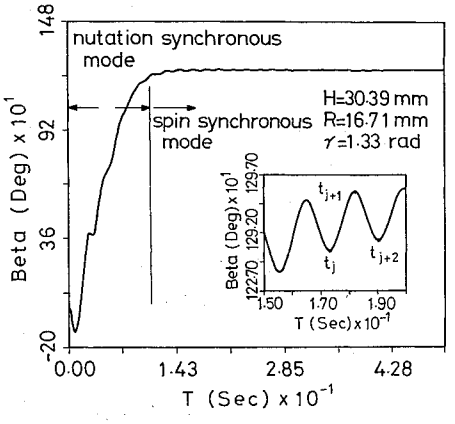

Fig. 4 Time history of the angular displacement of the mercury relative to the rotor.

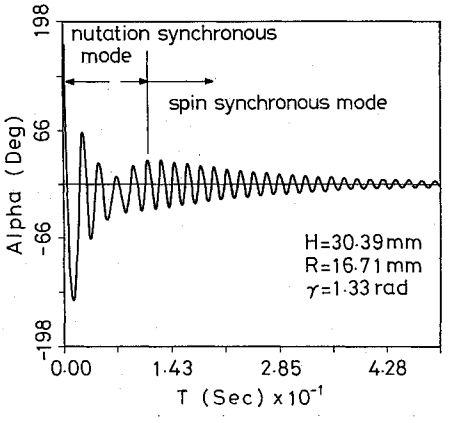

Fig. 5 Time history of the angle α.

where d is the diameter of the circular cross section. The d in Eq. (24) is replaced by $2(D + \Delta R)/\pi$ for the curved pipe with rectangular cross section. Equating the frictional force F_D to the shearing force which is obtained by multiplying the shear stress by the common contact area of the mercury slug and the ring, i.e.,

$$C_d R\dot{\beta} = 2(D + \Delta R)R\gamma\tau \tag{25}$$

we can evaluate the damping coefficient c_d. Substituting Eqs. (23) and (24) into Eq. (25) and using $\dot{\beta} \approx (\sigma - 1)\omega_z$,[2] one has

$$C_d = 0.0665\rho(D + \Delta R)\{[(D + \Delta R)\nu]/D\Delta R\}^{1/4}R\gamma \times [(\sigma - 1)R\omega_z]^{3/4} + 5.9 \times 10^{-3}\rho[(D + \Delta R)D\Delta R]^{1/2}R^{3/2}\gamma \times (\sigma - 1)\omega_z \tag{26}$$

where $\sigma = J_3/J$, and $J = J_1 = J_2$.

Numerical Results of Dynamic Analysis

Considering the special example for which $R = 16.71$ mm, $\Delta R = 1.4$ mm, $H = 30.39$ mm, $D = 0.78$ mm, $\gamma = 1.33$ rad, ρ (mercury) $= 13.6$ g/cm^3, $\nu = 0.00117$ cm^2/s, spin rate $\dot{\psi}(0) = 70$ Hz, $J_1 = J_2 = 400$ g $-$ cm^2, and $J_3 = 600$ g $-$ cm^2. Assume that the rotor is subjected to such an impulsive torque that $\omega_x(0) = 100$ rad/s and $\omega_y(0) = 0$ rad/s; the time history of nutation angle is shown in Fig. 3. As can be seen, the nutation angle descends drastically in the nutation-synchronous mode and then oscillates with small amplitude around a residual mean value in the spin-synchronous mode. Figure 4 is the time history of the angular displacement of the mercury relative to the rotor. The precession of the rotor is faster than its spin and is in the opposite direction since $J_3 > J$,[9] so the mercury is driven by precession and hence the u axis moves further and further away from the x axis; this is evidenced by the rapid growth of the β curve in the nutation-synchronous mode shown in Fig. 4. β almost remains constant in the spin-synchronous mode, which means that the mercury seems to synchronize with the rotor. This is because precession fades out and spin dominates as the nutation angle decays. Let us denote the plane formed by the angular momentum vector $\boldsymbol{h}$ and the z axis as the nutation plane. Then this nutation plane intersects the outer wall of the ring at two points E_1 and E_2, where E_1 is farther from $\boldsymbol{h}$ than E_2. Let α denote the angular displacement of the slug measured in the counterclockwise sense from the $O'E_1$ axis. Then Fig. 5 shows that the slug is entrapped into the nutation plane eventually due to the centrifugal inertia induced by the precession of the rotor around the vector $\boldsymbol{h}$. The average residual nutation angle as shown in Fig. 3 is about 0.56 deg. This result can be predicted theoretically as follows: On the assumption that the slug sticks to the rotor finally, due to the unbalanced mass of the crescent mercury, the inertia matrix of the gyroscope will be in the nondiagonal form as

$$I = I_m + I_g = \begin{bmatrix} I_1 + J & 0 & -I_4 \\ 0 & I_2 + J & 0 \\ -I_4 & 0 & I_3 + J_3 \end{bmatrix}$$

Let the u', v', z' coordinate axes be the principal axes of I and θ_ω the angle between the z' and z axes. Since $I_{z'u'}$ must be zero, i.e.,

$$I_{z'u'} = [-\sin\theta_\omega, 0, \cos\theta_\omega]I[\cos\theta_\omega, 0, \sin\theta_\omega]^T$$

one has

$$\tan 2\theta_\omega = \frac{2I_4}{J_3 - J + I_3 - I_1}$$

The value of θ_ω is found to be 0.578 deg and is in good agreement with the numerical result. Because a symmetric spinning body will have minimum kinetic energy if the spin

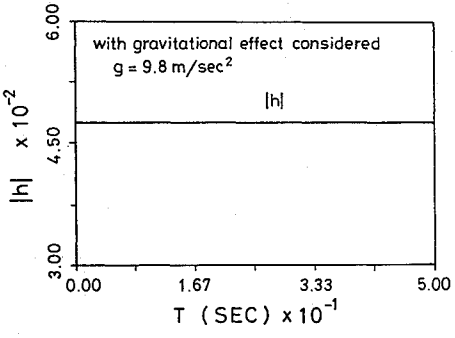

Fig. 6 Magnitude of h with gravitational effect considered.

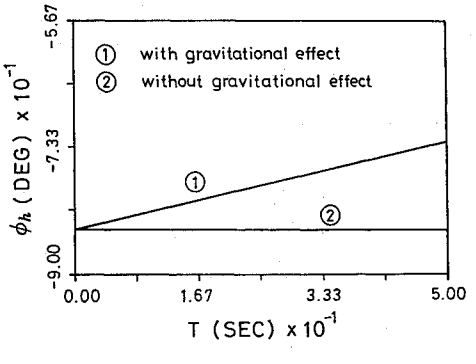

Fig. 7 Time history of the angle ϕ_h.

axis is the principal axis of maximum moment of inertia,[12] the rotor will therefore precess in the spin-synchronous mode around the z' axis that is aligned with the vector $\boldsymbol{h}$ and is at an angle θ_ω (the residual nutation angle) with the spin axis.

If the gravitational force of the mercury is taken into account, the angular momentum $\boldsymbol{h}$ of the gyroscope is no longer conserved. Let θ_h denote the angle between the vector $\boldsymbol{h}$ and the Z axis, and ϕ_h the precessional angular displacement of the vector $\boldsymbol{h}_{XY}$ measured from the X axis, where $\boldsymbol{h}_{XY}$ is the projection of the vector $\boldsymbol{h}$ on the XY plane. Our numerical results show that the magnitude of $\boldsymbol{h}$ is almost constant as shown in Fig. 6, and the value of θ_h is close to a small constant because the mass of mercury slug is much smaller than that of the rotor and because of the high spin rate of the rotor. Figure 7 shows that the vector $\boldsymbol{h}$ precesses around the Z axis with a very slow constant rate of 0.326 deg/s. From the above-mentioned results, the gravitational effect of the mercury on the angular momentum of the gyroscope is negligibly small, so it is neglected in the following parameter analysis.

Optimal Design

Optimization Problem

As long as the mercury behaves as a slug, the rotor inevitably has residual nutational motion. If the gyroscope is desired to track a target with minimum error, it is required that the nutation angle decays as rapidly as possible in the nutation-synchronous mode and the average residual nutation angle in the spin-synchronous mode is as small as possible. But a given system that has the character that the nutation angle decays faster in the nutation-synchronous mode will have

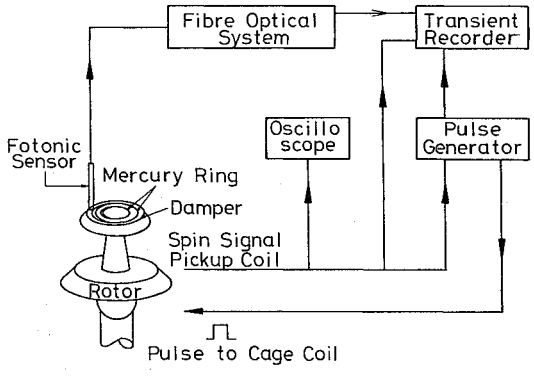

Fig. 8 Diagram of measuring system.

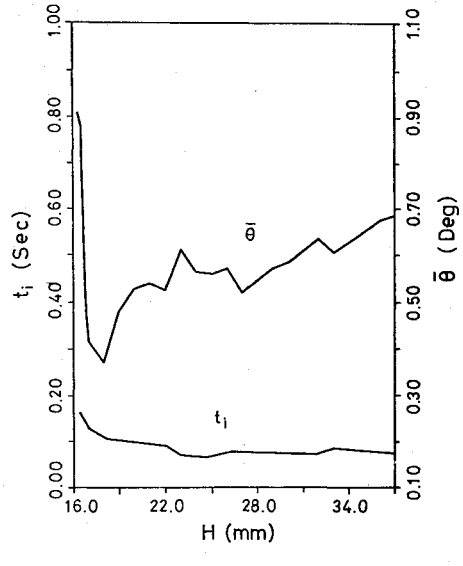

Fig. 9 Effect of H on t_i and $\bar{\theta}$.

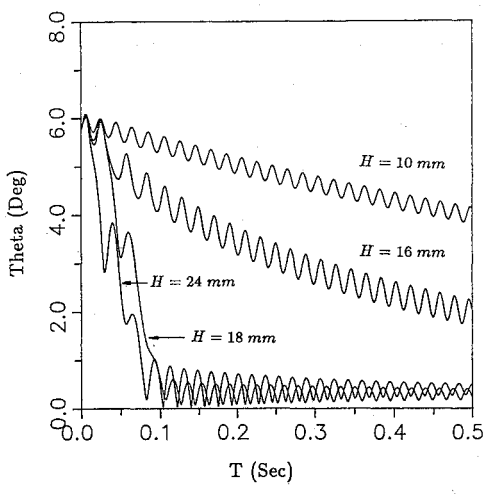

Fig. 10 Time history of θ for various H.

larger residual nutation angle in the spin-synchronous mode, and vice versa. So various compromises between them may be as needed for different design stratagems. The general form of the cost function ψ_0 for this optimization problem is chosen as

$$\psi_0 = c_1 t_i(\boldsymbol{b}) + c_2 t_f(\boldsymbol{b}) + \frac{c_3}{t_f - t_i}\int_{t_i}^{t_f} \theta(\boldsymbol{q};\boldsymbol{b})\, dt \tag{27}$$

where $\boldsymbol{q}[=(\omega_x, \omega_y, \omega_z, \beta, \dot{\beta})^T]$ is the vector of the state variables and θ is the nutation angle; t_i is the transition time from the nutation-synchronous mode to the spin-synchronous mode; t_f is the time elapsed in the spin-synchronous mode until the amplitude of the oscillatory nutation angle decays to reach a given criterion. Both t_i and t_f depend on system parameters. The third term of Eq. (27) is the average residual nutation angle in the interval $[t_i, t_f]$, and c_1, c_2, and c_3 are the desired weighting constants. The radius of the ring, the height of the damper to the center of mass of the gyroscope, and the angle of fill of the mercury are the primary parameters of the damper which have significant influence on the nutational motion. So they are designated as design variables; i.e., $\boldsymbol{b} = [H, R, \gamma]^T$. Then the optimization problems are formulated as follows:

Minimize

$$\psi_0[\boldsymbol{q}(t;\boldsymbol{b}), \boldsymbol{b}], \qquad t \in [0, t_f] \tag{28}$$

subject to

$$M(\boldsymbol{q}, \boldsymbol{b})\dot{\boldsymbol{q}} = f(\boldsymbol{q}, \boldsymbol{b}) \tag{29a}$$

and

$$\boldsymbol{b}^L \le \boldsymbol{b} \le \boldsymbol{b}^U \tag{29b}$$

where $\boldsymbol{b}^L$ and $\boldsymbol{b}^U$ are the lower and upper limits of $\boldsymbol{b}$, and Eq. (29b) is the compact form of Eq. (21). As to the transition from the nutation-synchronous mode to spin-synchronous mode, the transition time is difficult to be defined by definite equations; it is interpreted physically as the instant when the drag of the friction acted on the slug is balanced by the centrifugal inertia of the slug.[1,2] Alfriend[2] defined approximately the instant when the angular displacement of the slug relative to the nutation plane is reduced to the value of 90 deg; i.e., $\alpha = \pi/2$ as the transition time. But this condition is not applicable to our case for which the spin rate of the rotor is very high. Referring to Fig. 5, most of the time the angle α is less than $\pi/2$ and the change of motion behavior for these two modes is not so clear-cut as the β curve in Fig. 4 or the θ curve in Fig. 3 reveals. For less computational effort and carrying

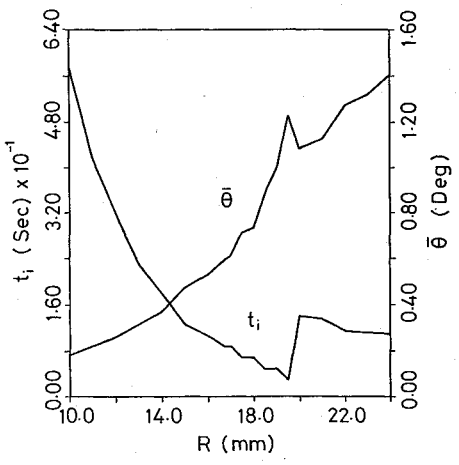

Fig. 11 Effect of R on t_i and $\bar{\theta}$.

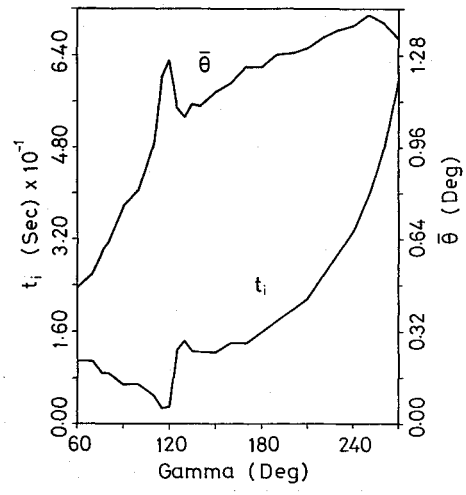

Fig. 12 Effect of γ on t_i and $\bar{\theta}$.

physical meaning, the suitable logical constraints based on the θ curve are exploited as an expedient to locate the t_i approximately; i.e.,

$$\dot{\theta}(t_i;\, \boldsymbol{b}) = 0 \tag{30a}$$

and

$$\theta(t_i;\, \boldsymbol{b}) \leq 0.8 \text{ deg} \tag{30b}$$

Based on the β curve shown in Fig. 4, the expedient way for determining t_f are the following logical constraints:

$$\dot{\beta}(t_j) = \dot{\beta}(t_{j+1}) = \dot{\beta}(t_{j+2}) = 0 \tag{31a}$$

and

$$\|\beta(t_{j+2}) - \beta(t_{j+1})| - |\beta(t_{j+1}) - \beta(t_j)\| < \epsilon \tag{31b}$$

where ϵ is a small positive real number and it is assigned a value of 1 deg in this paper. The instant time t_j at which Eqs. (31) are satisfied is designated as t_f. Equations (31) mean that at the time t_f the decay rate of the nutation angle in the spin-synchronous mode slows down to a small desired value.

Design Sensitivity Analysis

The purpose of design sensitivity analysis is to obtain the derivatives of the state variables, the cost function, and the performance constraints with respect to the design variables. Those derivatives will then be used to calculate the improved design in the optimization process. Using direct differentiation and the Leibnitz rule, the $d\psi_0/d\boldsymbol{b}$ is

$$\frac{d\psi_0}{d\boldsymbol{b}} = c_1 \frac{dt_i}{d\boldsymbol{b}} + c_2 \frac{dt_f}{d\boldsymbol{b}} - \frac{c_3}{(t_f - t_i)^2}\int_{t_i}^{t_f} \theta \, dt \left[\frac{dt_f}{d\boldsymbol{b}} - \frac{dt_i}{d\boldsymbol{b}}\right]$$
$$+ \frac{c_3}{t_f - t_i}\left\{\int_{t_i}^{t_f} (\theta_q q_b + \theta_b)\, dt + \frac{dt_f}{d\boldsymbol{b}}\theta(q;\, \boldsymbol{b})\Big|_{t_f} - \frac{dt_i}{d\boldsymbol{b}}\theta(q;\, \boldsymbol{b})\Big|_{t_i}\right\} \tag{32}$$

For the system having few design variables, the direct differentiation method[13] is more efficient than the adjoint variable method[14] in solving the variables q_b. Define the first-order variation of q and $\dot{q}$ due to the variation of $\boldsymbol{b}$ as

$$\delta q = q_b \delta \boldsymbol{b} \tag{33}$$

$$\delta \dot{q} = \dot{q}_b \delta \boldsymbol{b} \tag{34}$$

Then the variation of equations of motion due to $\delta \boldsymbol{b}$ is

$$(M\dot{q})_{\dot{q}} \delta \dot{q} + (M\dot{q})_q \delta q + (M\dot{q})_b \delta \boldsymbol{b} = f_q \delta q_b + f_b \delta \boldsymbol{b} \tag{35}$$

The substitution of Eqs. (33) and (34) into Eq. (35) yields

$$[M\dot{q}_b + (M\dot{q})_q q_b + (M\dot{q})_b]\, \delta \boldsymbol{b} = [f_q q_b + f_b]\, \delta \boldsymbol{b} \tag{36}$$

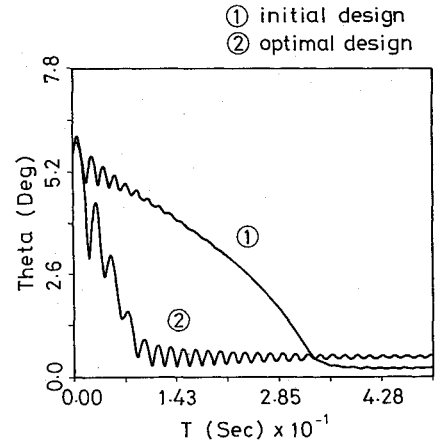

Fig. 13 Nutation angle behavior of initial design and optimal design.

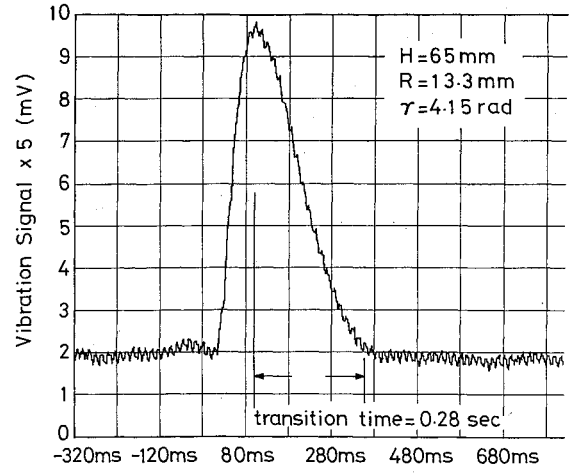

Fig. 14 Vibration signal of nutation and precession.

Equation (36) holds for arbitrary $\delta \boldsymbol{b}$, so one obtains the differential equation for dependent variables $\boldsymbol{q}_b$ in the form as

$$M\dot{\boldsymbol{q}}_b = f_q \boldsymbol{q}_b + f_b - (M\dot{\boldsymbol{q}})_q \boldsymbol{q}_b - (M\dot{\boldsymbol{q}})_b \tag{37}$$

Equation (37) is linear in variables $\boldsymbol{q}_b$ but nonlinear in state variables $\boldsymbol{q}$, so it is better to solve Eqs. (21) and (37) simultaneously. The total variation of Eq. (30a) due to the variations $\delta \boldsymbol{b}$ and δt_i is

$$\delta\dot{\theta}(t_i;\, \boldsymbol{b}) = \dot{\theta}_b\, \delta \boldsymbol{b} + \frac{\mathrm{d}\dot{\theta}}{\mathrm{d}t}\bigg|_{t_i} \delta t = 0 \tag{38}$$

Substituting $\delta t_i = t_{ib}\delta \boldsymbol{b}$ into Eq. (38), one obtains

$$\frac{\mathrm{d}t_i}{\mathrm{d}\boldsymbol{b}} = -\frac{\dot{\theta}_b(t_i)}{\ddot{\theta}(t_i)} \tag{39}$$

The same procedure can be applied to Eq. (31a) to obtain the quantity $\mathrm{d}t_f/\mathrm{d}\boldsymbol{b}$ in the similar form as

$$\frac{\mathrm{d}t_f}{\mathrm{d}\boldsymbol{b}} = -\frac{\dot{\beta}_b(t_f)}{\ddot{\beta}(t_f)} \tag{40}$$

The remaining unknowns of Eq. (32) are θ_q and θ_b. From the geometric relation, the nutation angle can be obtained by the following equation:

$$\tan\theta = \frac{h_t}{h_s} \tag{41}$$

where h_t and h_s are the transverse and spin angular momentums of the gyroscope, respectively. The differentiation of Eq. (41) with respect to $\boldsymbol{q}$ yields

$$\theta_q = [(h_t)_q h_s - h_t(h_s)_q]/(h_s^2 + h_t^2) \tag{42}$$

Following the same procedure, one obtains

$$\theta_b = [(h_t)_b h_s - h_t(h_s)_b]/(h_s^2 + h_t^2) \tag{43}$$

Optimization

There are several excellent optimization algorithms in existence. In this research, the linearization method[15] based on a technique proposed by Pshenichny and Danilin[16] is employed. This method has been proved to be globally convergent[16] and is guaranteed to converge to at least one local optimum for any initial design. The basic idea of this gradient-based algorithm is to obtain the direction vector for the change in design by solving a quadratic programming problem invoking linearized cost and constraints. Subsequently, the magnitude of the design change along this direction is estimated according to the amount of cost reduction and constraint-violation correction.

Experimental Test

An experiment was conducted to verify the behavior of nutation angle. The diagram of the measuring system is shown in Fig. 8. A small coil is placed beside the rotor-driving coil to pick up the spin rate of the gyro. This signal was also used to trigger the pulse generator to generate a single square wave. This pulse was applied to the caging coil to produce a magnetic torque to the rotor so that the rotor is in motion with large nutation angle. A fiber-optical displacement system[17] was used to measure the response of the rotor. This response recorded is a combination of nutation and precession of the rotor.

Results and Discussion

The initial value problem of Eqs. (21) and (37) are integrated numerically by the subroutine DE.[18] The values of t_i and $\bar{\theta}$ [the average residual nutation angle defined by the third term in Eq. (27)] are plotted as functions of H with γ and R fixed in Fig. 9. Increasing H will decrease t_i, and decrease $\bar{\theta}$ first and then increase it slowly. For the same initial conditions and the same parameters except H, Fig. 8 shows the effect of H on the t_i as well as the behavior of the nutation angle. It is clear that a bifurcation point occurs at about $H = 16$ mm. When H is less than 16 mm, only the spin-synchronous mode exists. This means that in order to remove the nutational motion of the rotor more effectively the value of H must be large enough so as to have the slug captured in the nutation-synchronous mode. This bifurcation point is of particular importance for practical design and is not mentioned in the existing literature. The fact that H affects t_i implies that H influences the decay time constant of the nutation-synchronous mode, but the influence is not much according to the small slope of the t_i curve shown in Fig. 9 and the small difference between the t_i for $H = 18$ mm and the t_i for $H = 24$ mm shown in Fig. 10. So the time constant for the nutation-synchronous mode seems to be independent of H in an approximate sense. The expression for the nutation angle in the spin-synchronous mode obtained by Alfriend[2] does not reveal the existence of the residual nutation angle as time goes to infinity. But the residual nutation angle indeed exists and it can be proved as follows. In the spin-synchronous mode, the slug is almost synchronized to the rotor, i.e., $\beta \approx 0$. Substituting this result into Eqs. (21) and (B1–B4) and setting $\dot{\omega}_x$, $\dot{\omega}_y$, $\dot{\omega}_z$, $\dot{\beta}$, and $\ddot{\beta}$ to be zero, the equilibrium point $(\omega_x, \omega_y, \omega_z, \beta) = (\omega_{xe}, \omega_{ye}, \omega_{ze}, 0)$ will satisfy the following equations:

$$\omega_{ye}\{-[I_3 + I_2]\omega_{ze} + I_4\omega_{xe}\} = 0 \tag{44}$$

$$[I_3 - I_1]\omega_{xe}\omega_{ze} - I_4\omega_{xe}^2 + I_4\omega_{ze}^2 = 0 \tag{45}$$

$$\omega_{ye}[(I_1 - I_2)\omega_{xe} - I_4\omega_{ze}] = 0 \tag{46}$$

From Eqs. (44) and (46), we have that $\omega_{ye} = 0$. From Eq. (45), we have that $\omega_{xe} \neq 0$ since ω_{ze} is almost constant in the spin-synchronous mode. Then from Eq. (41) we know that the residual nutation angle is not zero at the final state because of $\omega_{xe} \neq 0$. In order to acquire the more correct residual nutation angle, the equations obtained by approximating the exact equations of motion up to terms of $\mathcal{O}(\epsilon^1)$ rather than terms of $\mathcal{O}(\epsilon^0)$ (as done by Alfriend) may be as needed. But these equations are nonlinear and are too involved to yield closed-form solutions. Therefore based on the exact equations of motion, finding the optimum damper parameters through the optimization method is developed systematically in this paper. The results obtained by Cartwright et al.[1] about the transition time t_i showed that the transition time t_i increases as H increases, because $(\partial t_i/\partial H) \propto (1/H^3) > 0$. Their result is contrary to ours. However, by intuition the increase of H will increase the velocity of the wall of the ring, which in turn will increase the velocity of the mercury relative to the rotor and hence speed up the damping of nutational motion of the rotor. The values of t_i and $\bar{\theta}$ are plotted as functions of R with H and γ fixed in Fig. 11. As can be seen, increasing the value of R reduces the value of t_i but increases $\bar{\theta}$. Increasing R will increase the distance of the center of mass of the crescent mercury to the spin axis and hence increase the centrifugal inertia due to spin, which in turn increases $\bar{\theta}$. Also, the increase of R increases the distance of the center of mass of the mercury to the angular momentum vector $\boldsymbol{h}$ and hence enlarges the centrifugal inertia due to precession, which in turn drives the slug much out of synchronizing with the rotor and to move more closely to the nutation plane. In other words, the increase of R enhances the relative motion between the rotor and the mercury and thus accelerates the damping of nutational motion; so the value of t_i is reduced. The effects of the angle of fill γ on the t_i and $\bar{\theta}$, with H and R fixed, are shown in Fig. 12. As the figure shows, t_i decreases for the value of γ below 120 deg and increases after that, and the average residual nutation angle rises as γ increases. The centrifugal inertia f_c of the

Table 1 Optimal design for various $\omega_u(0)$ and $\omega_v(0)$

Initial conditions			Optimal design		
ω_u, rad/s	ω_v, rad/s	ω_z, rad/s	H, mm	R, mm	γ, rad
80	0	628	30.19	15.81	1.28
100	0	628	30.23	16.49	1.33
120	0	628	29.98	16.26	1.38
140	0	628	30.62	16.38	1.36
100	20	628	29.80	16.12	1.39

Table 2 Optimal design for various $\beta(0)$ and $\dot{\beta}(0)$

Initial conditions		Optimal design		
β, deg	$\dot{\beta}$, rad/s	H, mm	R, mm	γ, rad
45	0	30.14	16.46	1.32
90	0	30.14	16.46	1.32
0	40	29.85	16.71	1.26
0	−40	30.17	16.27	1.41
45	40	30.37	16.33	1.27
0	80	30.15	16.59	1.28

mercury due to spin is proportional to the mass of the mercury slug m and proportional to the square of the distance r of the center of mass of the mercury to the spin axis, i.e., $f_c \propto mr^2$. The increase of γ increases the value of m but decreases the value of $r[= R \sin(\gamma/2)/(\gamma/2)]$. However, the net centrifugal inertia due to spin increases so that $\bar{\theta}$ rises. This can be seen by expanding $\sin(\gamma/2)$ to obtain that $f_c \propto [(\gamma/4) - (\gamma^3/48) + \cdots] > 0$ and $(\partial f_c/\partial\gamma) \propto [(1/4) - (\gamma^2/16) + \cdots] > 0$ for $\gamma \le \pi/2$. Since these parameters affect the decay of nutational motion in their own way, the determination of the best parameters through optimization seems reasonable and necessary.

The lower and upper limits of $\boldsymbol{b}$ are chosen as $\boldsymbol{b}^L = (15.0, 5.0, 1.0)^T$ and $\boldsymbol{b}^U = (40.0, 20.0, 6.0)^T$, respectively. For the given initial design $\boldsymbol{b}^0 = (26.5, 10.15, 2.0)^T$, the optimal design is found to be $\boldsymbol{b} = (30.39, 16.71, 1.33)^T$. Figure 13 shows that the t_i of the optimal design is reduced to one third of that of the initial design but the average residual nutation angle of the optimal design is a little larger than that of the initial design. The dimensions of the ring damper for experimental test are $H = 65$ mm, $R = 13.3$ mm, $\gamma = 4.15$ rad. Figure 14 shows the vibration signal of the rotor output from the Fotonic sensor. The transition time is about 0.28 s and its order of magnitude is the same as those of the initial and optimal designs shown in Fig. 13.

Since initial conditions influence system responses, the transition time t_i is therefore affected by initial conditions besides system parameters, so does the cost function ψ_0. The optimal design will be useful only if it is independent of or insensitive to the initial conditions. The effects of different $\omega_u(0)$, $\omega_v(0)$, $\beta(0)$, and $\dot{\beta}(0)$ on the optimal design are shown in Table 1 and Table 2. It is found that the optimal design is insensitive to those initial conditions, which means that for each set of initial conditions the damper parameters influence the cost function ψ_0 (the damper performance) in the same trend.

Conclusions

The dynamics and design of a mercury-filled ring damper for a freely precessing body are analyzed. The good agreement on the transition time from the nutation-synchronous mode to the spin-synchronous mode between the theoretical prediction and experimental result validates our modeling. The effects on the decay of nutation angle and the residual nutation angle in the spin-synchronous mode are quite different for various parameters of the damper; it may be positive or negative. Therefore, the best choice of the design parameters is obtained through solving the optimization problem that minimizes the time elapsed in the nutation-synchronous mode and the average residual nutation angle in the spin-synchronous mode. The logical constraints are used to overcome the difficulty in finding the transition time. The direct differentiation method is applied to the complete nonlinear equations of motion to evaluate the gradients of the state variables with respect to design variables. The result shows that the decay of the nutation angle has been accelerated to a great extent if the damper is designed optimally.

Appendix A

The moments of inertia of the mercury about the point o in the u,v,z coordinate system are given as following:

$$I_{uu} = \int (v^2 + z^2)\, dm = 2\int_0^{\gamma/2} (R^2 \sin^2\theta + H^2)\frac{m}{\gamma}\, d\theta = m\left[H^2 + \frac{R^2}{2}(1 - K)\right]$$

where $m = \gamma RD\rho\Delta R$ and ρ is the density of the mercury,

$$I_{vv} = m\left[H^2 + \frac{R^2}{2}(1 + K)\right], \qquad I_{zz} = mR^2$$

$$I_{uv} = I_{vu} = 0, \qquad I_{vz} = I_{zv} = 0$$

$$I_{uz} = I_{zu} = mRHK$$

The nonzero elements of the matrix I_m are redefined as

$$I_1 = I_{uu}, \qquad I_2 = I_{vv}, \qquad I_3 = I_{zz}, \qquad I_4 = I_{uz}$$

Appendix B

The gravity is assumed to lie in the negative z axis. The f_1, f_2, f_3, and f_4 of Eq. (22) are given as

$$\begin{aligned} f_1 = {} & (I_1 - I_2)\sin\beta\cos\beta\omega_x\omega_z - [I_3 + J_2 - J_1 + I_1\sin^2\beta \\ & + I_2\cos^2\beta]\omega_y\omega_z + I_4\cos\beta\omega_x\omega_y + I_4\sin\beta\omega_y^2 \\ & - I_4\sin\beta\omega_z^2 + 2(I_1 - I_2)\sin\beta\cos\beta\dot{\beta}\omega_x - I_4\sin\beta\dot{\beta}^2 \\ & - 2I_4\sin\beta\dot{\beta}\omega_z - [(I_1 - I_2)(\cos^2\beta - \sin^2\beta) + I_3]\dot{\beta}\omega_y \\ & - mgRk\sin\beta e_0^2 + mgRk\sin\beta e_1^2 + mgRk\sin\beta e_2^2 \\ & - mgRk\sin\beta e_3^2 + 2mgae_1e_0 + 2mgae_2e_3 \end{aligned} \tag{B1}$$

$$\begin{aligned} f_2 = {} & -(I_1 - I_2)\sin\beta\cos\beta\omega_y\omega_z + [-J_1 + J_2 + I_3 \\ & - I_1\cos^2\beta - I_2\sin^2\beta]\omega_x\omega_z - I_4\sin\beta\omega_x\omega_y - I_4\cos\beta\omega_x^2 \\ & + I_4\cos\beta\omega_z^2 - 2(I_1 - I_2)\sin\beta\cos\beta\dot{\beta}\omega_y + I_4\cos\beta\dot{\beta}^2 \\ & + 2I_4\cos\beta\dot{\beta}\omega_z + [(I_3 - (I_1 - I_2)(\cos^2\beta - \sin^2\beta)]\dot{\beta}\omega_x \\ & + mgRk\cos\beta e_0^2 - mgRk\cos\beta e_1^2 - mgRk\cos\beta e_2^2 \\ & + mgRk\cos\beta e_3^2 + 2mgae_0e_2 - 2mgae_1e_3 \end{aligned} \tag{B2}$$

$$\begin{aligned} f_3 = {} & (I_1 - I_2)(\cos^2\beta - \sin^2\beta)\omega_x\omega_y - (I_1 - I_2)\sin\beta\cos\beta \\ & \times(\omega_x^2 - \omega_y^2) + 2mgRk\sin\beta(e_1e_3 - e_0e_2) - 2mgRk\cos\beta \\ & \times(e_0e_1 - e_2e_3) + I_4\sin\beta\omega_x\omega_z - I_4\cos\beta\omega_y\omega_z \end{aligned} \tag{B3}$$

$$\begin{aligned} f_4 = {} & (I_1 - I_2)(\cos^2\beta - \sin^2\beta)\omega_x\omega_y - (I_1 - I_2)\sin\beta\cos\beta \\ & \times(\omega_z^2 - \omega_y^2) - 2mgRk\cos\beta(e_2e_3 - e_0e_1) + 2mgRk\sin\beta \\ & \times(e_1e_3 - e_0e_2) + I_4\sin\beta\omega_x\omega_z - I_4\cos\beta\omega_y\omega_z - C_dR^2\dot{\beta} \end{aligned} \tag{B4}$$

Acknowledgments

The authors wish to acknowledge the support of the Chung Shan Institute of Science and Technology, Republic of China, and the constructive suggestions of K. T. Alfriend and the reviewers.

References

[1]Cartwright, W. F., Massingill, E. C., and Trueblood, R. D., "Circular Constraint Nutation Damper," *AIAA Journal,* Vol. 1, No. 6, 1963, pp. 1375–1380.

[2]Alfriend, K. T., "Partially Filled Viscous Ring Nutation Damper," *Journal of Spacecraft and Rockets,* Vol. 11, No. 7, 1974, pp. 456–462.

[3]Alfriend, K. T., and Spencer, T. M., "Comparison of Filled and Partially Filled Nutation Damper," *Journal of the Aeronautical Sciences,* Vol. XXXI, No. 2, 1983, pp. 198–202.

[4]Bhuta, P. G., and Koval, L. R., "A Viscous Ring Damper for a Freely Precessing Satellites," *International Journal of Mechanical Sciences,* Vol. 8, 1966, pp. 383–395.

[5]Miles, J. W., "On the Annular Damper for a Freely Precessing Gyroscope—II," *Journal of Applied Mechanics,* Vol. 30, June 1963, pp. 189–192.

[6]Whittaker, E. T., *A Treatise on the Analytical Dynamics of Particles and Rigid Bodies,* 4th ed., Cambridge University Press, New York, 1937, Chap. 1.

[7]Goldstein, H., *Classical Mechanics,* 2nd ed., Addison Wesley, 1980, Chap. 4, pp. 148–157.

[8]Nikravesh, P. E., *Computer-Aided Analysis of Mechanical Systems,* 1st ed., Prentice-Hall, Englewood Cliffs, NJ, 1988, Chap. 6, pp. 167–175.

[9]Meirovitch, L., *Methods of Analytical Dynamics,* McGraw-Hill, New York, 1970, Chap. 4, pp. 157–160.

[10]Cheng, K. C., Lin, R. C., and Ou, J. W., "Fully Development Laminar Flow in Curved Rectangular Channels," *Journal of Fluids Engineering,* Vol. 98, No. 1, 1976, pp. 41–48.

[11]Schlichting, H., *Boundary-Layer Theory,* 7th ed., McGraw-Hill, New York, 1969, Chap. XX, pp. 560–592.

[12]Wrigley, W., Hollister, W. M., and Denhard, W. G., *Gyroscopic Theory, Design, and Instrumentation,* The M.I.T. Press, Cambridge, MA, 1969, pp. 56–58.

[13]Chang, C. O., and Nikravesh, P. E., "Optimal Design of Mechanical Systems with Constraint-Violation Stabilization Method," *Journal of Mechanisms, Transmissions, and Automation in Design,* Vol. 107, No. 4, 1985, pp. 493–498.

[14]Haug, E. J., and Arora, J. S., *Applied Optimal Design,* Wiley, New York, 1979, pp. 330–353.

[15]Choi, K. K., Haug, E. J., Hou, J. W., and Sohoni, V. N., "Pshenichny's Linearization Method for Mechanical System Optimization," *ASME Journal of Mechanisms, Transmissions, and Automation in Design,* Vol. 105, No. 1, 1983, pp. 97–103.

[16]Pshenichny, B. N., and Danilin, Y. M., *Numerical Method in Extremal Problem,* MIR Publisher, Moscow, 1978, pp. 188–219.

[17]Cook, P. O., and Hamm, C. W., "Fiber-Optic Level Displacement Transducer," *Applied Optics,* Vol. 18, No. 19, 1979, pp. 320–324.

[18]Shampine, L. F., and Gordon, M. K., *Computer Solution of Ordinary Differential Equations,* 1st ed., W. S. Freeman, San Francisco, 1975, Chap. 10, pp. 156–223.